

## Different Thermal and Solubility Properties with Identical Crystal Structure - Case of Lenalidomide Hydrate

Qi Zhang<sup>a</sup>, Yitong Zhu<sup>a</sup>, Yisheng Xu<sup>a</sup>, Huaiyu Yang<sup>b,\*</sup>, Wei Li<sup>b</sup>, Xiangyang  
Zhang<sup>a,\*</sup>

<sup>a</sup> State Key Laboratory of Chemical Engineering, East China University of  
Science and Technology, Shanghai, 200237, China

<sup>b</sup> Department of Chemical Engineering, Loughborough University,  
Loughborough, LE11 3TU, UK

\*Corresponding authors.

### Supporting Information

#### 1. Solubility properties of crystals B, E1 and E2

The vitro studies of three LDM hydrates have been conducted at 37°C to evaluate the solubility properties by powder dissolution measurement. 0.5 mL of the samples were withdrawn at predetermined time intervals and were filtered immediately with a 0.22 μm syringe filter for HPLC determination. The samples were recovered and characterized by both PXRD and DSC. Fig. S1 shows that there is no transformation occurred before and after the powder dissolution measurement proved by both PXRD and DSC.

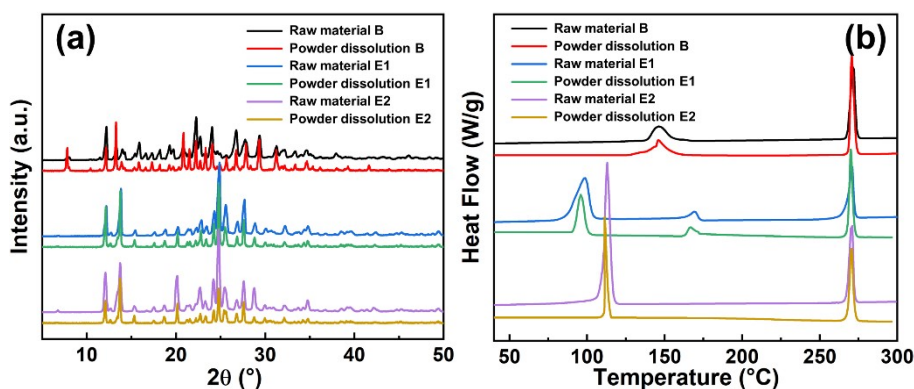


**Fig. S1.** LDM identification of powder dissolution measurement: (a) PXRD patterns and  
(b) DSC curves.

## 2. Thermal property and crystal structure of LDM Form B

Form B is the commercial hemihydrate of LDM, and its thermal properties were compared with those of crystals E1 and E2, as shown in Fig. S2. In the TGA curve, the weight loss during heating and dehydration confirmed Form B as a hemihydrate, amounting to about 3.3%. Form B had an initial peak at 146°C in DSC curve, indicating the loss of hydrated water molecules. The melting point of Form B was 270 °C, which was considered to be the same as the melting points of E1 and E2. In addition, single-crystal structure data of B with E1 and E2 were compared, as shown in Table S1.

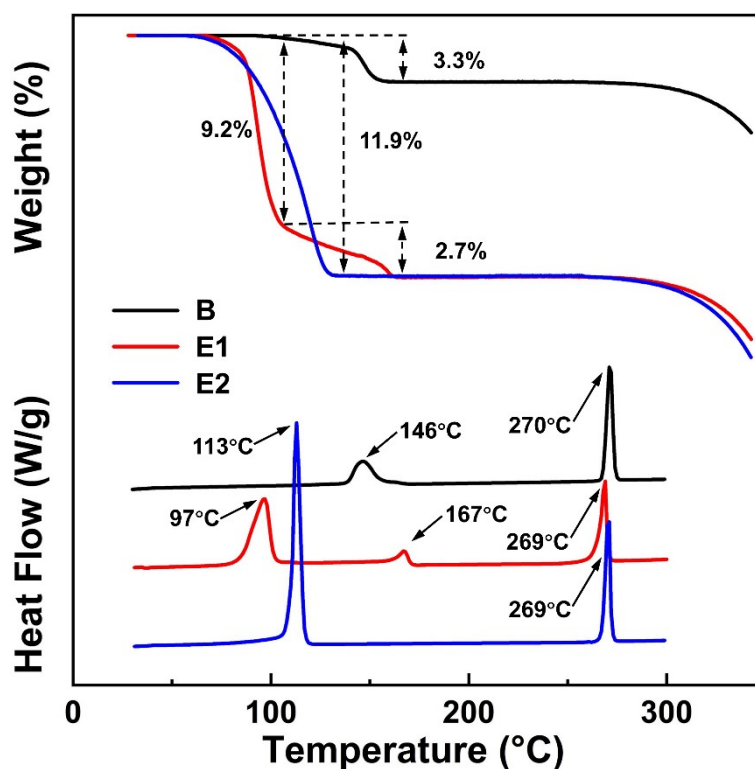


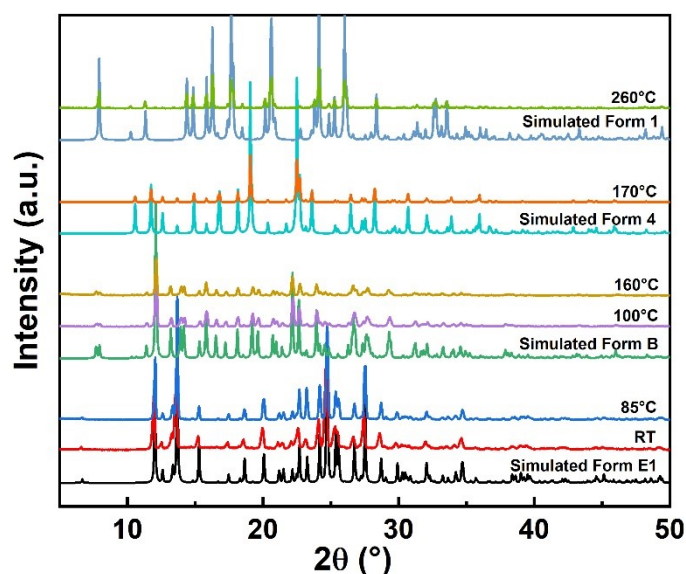
Fig. S2. TGA and DSC curves of LDM crystals B, E1 and E2.

**Table S1.** Single-crystal structure data of LDM B, E1 and E2.

Parameters	B	E1	E2
Formula	$C_{13}H_{13}N_3O_3 \cdot 0.5H_2O$	$C_{13}H_{13}N_3O_3 \cdot 2H_2O$	
Weight	268.29	295.29	
Crystal system	Monoclinic		
Space group	$P2_1/c$		
<i>a</i> (Å)	8.4425(7)	13.4400(3)	13.4569(3)
<i>b</i> (Å)	22.2874(19)	8.8402(2)	8.8327(2)
<i>c</i> (Å)	13.6627(12)	11.7381(3)	11.7392(3)
$\alpha$ (°)	90	90	90
$\beta$ (°)	101.0690(10)	99.1610(10)	99.2310(10)
$\gamma$ (°)	90	90	90
Z, Z'	8, 2	4, 1	4, 1
Volume (Å <sup>3</sup> )	2523.0(4)	1376.84(6)	1377.33(6)
CCDC NO.	755983	2289868	2383285

### 3. Polymorph transformation of LDM hydrates during dehydration

To identify the polymorphs of crystals E1 and E2 during the dehydration process, the experimental PXRD patterns at different temperatures were matched with the simulated patterns, shown in Figs. S3-S4. The simulated standard PRXD patterns were determined from the single-crystal structures, which have been reported for Forms 1, 4, and B<sup>1,2</sup>, corresponding to the CCDC numbers with 755982, 1487162, and 755983, respectively.

**Fig. S3.** Comparison of PXRD patterns of crystals E1 during the dehydration process.

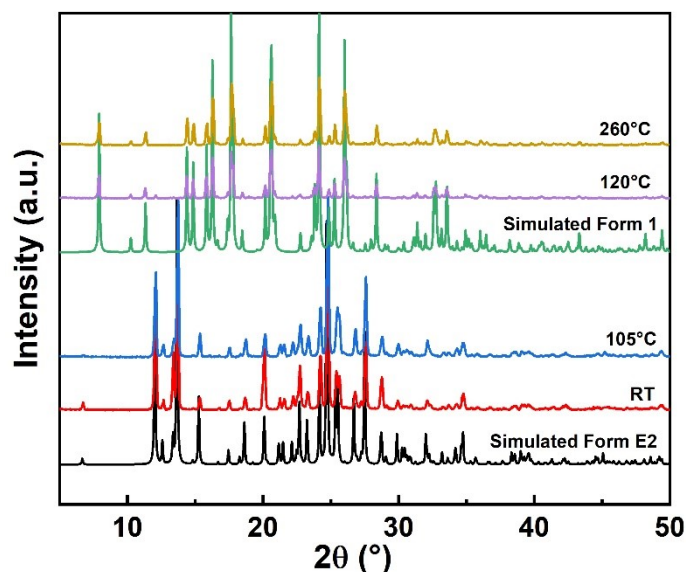


**Fig. S4.** Comparison of PXRD patterns of crystals E2 during the dehydration process.

#### 4. Polymorph identification of bulk and single crystals of E1 and E2

To obtain high-quality single crystals, we slightly varied the crystallization method, which differed slightly from the preparation procedures for bulk crystals. Fig. S5 shows the comparison of PXRD patterns of LDM E1 and E2 for the bulk crystals, single crystals and simulation. For both E1 and E2, the diffraction peak positions are the same in bulk-crystal, single-crystal and simulated PXRD patterns, indicating the same polymorph.

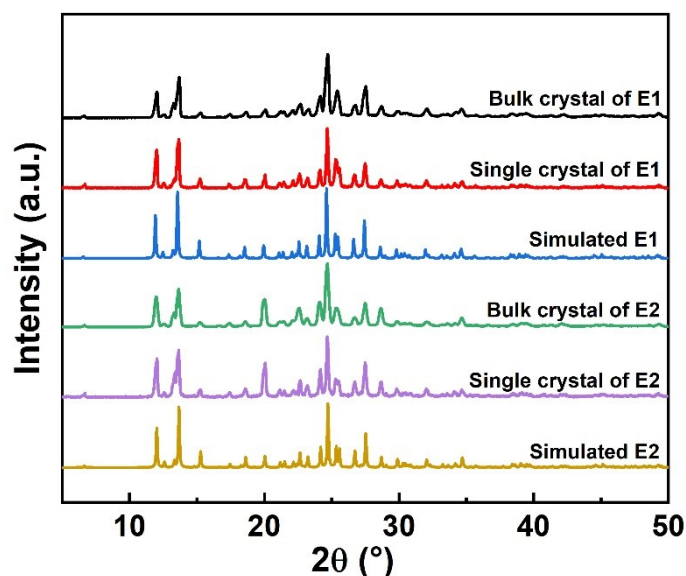


**Fig. S5.** Comparison of PXRD patterns of LDM E1 and E2 for the bulk crystals, single crystals and simulation.

## 5. Comparison of PXRD patterns of crystals E1 and E2

To compare the lattice orientation, PXRD patterns of crystals E1 and E2 were overlaid. The characteristic peaks were labeled by the Miller indices, and the intensity ( $I$ ) of these peaks were compared, as shown in Table S2. The simulated PXRD pattern of crystals E2 was also calculated by March-Dollase model in the preferred orientation of (1 0 0), as shown Fig. S6.

**Table S2.** Miller indices and intensity changes ( $\Delta I$ ) of characteristic peaks for LDM crystals E1 and E2.

$2\theta$ ( $^\circ$ )	Miller index	$I$ (%)		$\Delta I$ (%)
		E1	E2	
20.0	(3 0 0)	11.4	45.0	+33.6
24.0	(2 2 0)	22.2	35.8	+13.6
24.6	(2 2 -1)	100	100	0.0
25.4	(3 1 -2)	38.1	24.8	-13.3
27.5	(2 2 -2)	47.2	36.2	-11.0
28.7	(4 1 0)	15.1	28.2	+13.1

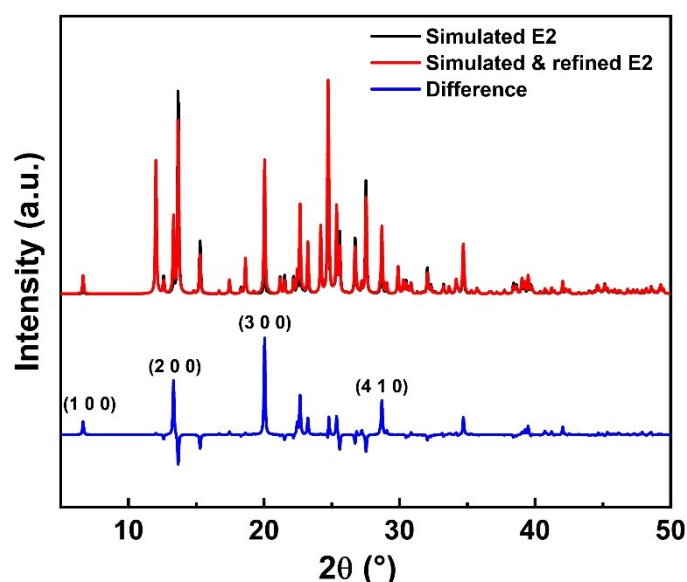


**Fig. S6.** Comparison of simulated PXRD pattern of crystals E2 under the preferred orientation in (1 0 0).

## 6. TGA determination for the dehydration kinetics of crystals E1 and E2

Based on the FWO method, TGA data of LDM crystals E1 and E2 were measured at different heating rates to explore the kinetics parameters and dehydration processes, shown in Figs. S7-S8.

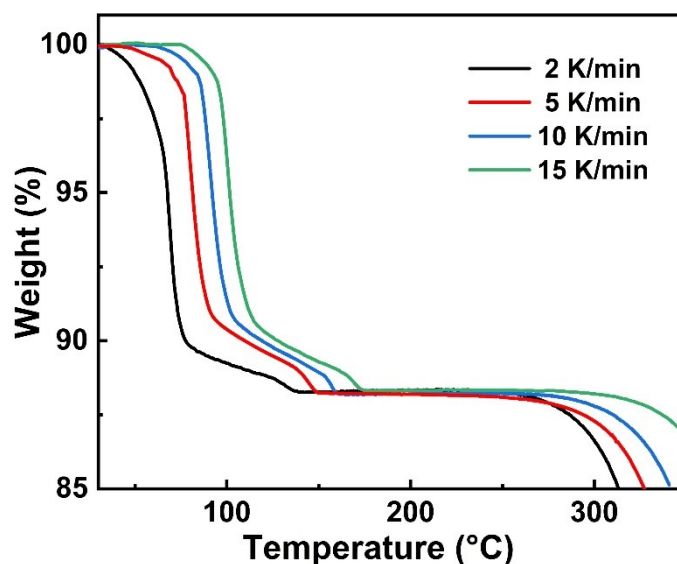


Fig. S7. TGA curves at different heating rates of LDM crystals E1.

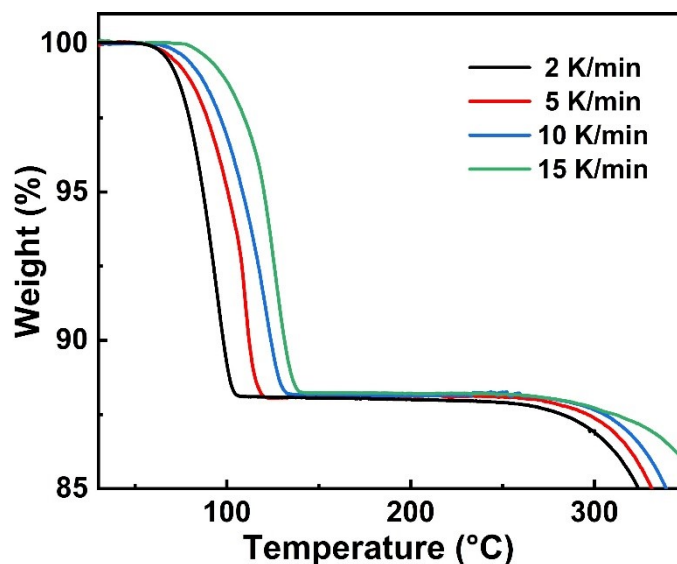


Fig. S8. TGA curves at different heating rates of LDM crystals E2.

## References

1. R. Chennuru, P. Muthudoss, R. S. Voguri, S. Ramakrishnan, P. Vishweshwar, R. R. C. Babu and S. Mahapatra, *Crystal Growth Des.*, 2017, 17, 612-628.
2. K. Ravikumar and B. Sridhar, *Acta. Crystallogr. C.*, 2009, 65, o502-o505